

GPU-Accelerated SPOCK for Scenario-Based Risk-Averse Optimal Control Problems*

Ruairi Moran[†], Pantelis Sopasakis[†]

June 11, 2025

Abstract

This paper presents a GPU-accelerated implementation of the SPOCK algorithm, a proximal method designed for solving scenario-based risk-averse optimal control problems. The proposed implementation leverages the massive parallelization of the SPOCK algorithm, and benchmarking against state-of-the-art interior-point solvers demonstrates GPU-accelerated SPOCK’s competitive execution time and memory footprint for large-scale problems. We further investigate the effect of the scenario tree structure on parallelizability, and so on solve time.

1 Introduction

Risk-averse optimal control problems (RAOCs) have a wide variety of applications, e.g., in MPC [1] for microgrids [2], in reinforcement learning [3], [4], for energy management systems [5], air-ground rendezvous [6], and collision avoidance [7], [8].

In this work, the term *risk* refers to the uncertainty of the detrimental effect of future events, and the term *risk-averse* is used to describe a preference for outcomes with reduced uncertainty of this detrimental effect.

The two main paradigms for approaching risk represent perspectives of the future. The *stochastic/risk-neutral* paradigm represents the naive perspective that the future will unfold as expected. The *robust/worst-case* paradigm represents the conservative perspective that the future will unfold in the worst possible way. In terms of formulating optimal control problems (OCPs) for uncertain

systems, the risk-neutral approach assumes that we have perfect information about the distributions of the involved random disturbances [9]. The robust approach ignores any statistical information that is usually available [10, Ch. 3].

The modern risk-averse paradigm forms a bridge between the risk-neutral and worst-case paradigms [11, Ch. 8]. The risk-averse formulation takes into account *inexact* and *data-driven* statistical information [12] using risk measures. A *risk measure* quantifies the magnitude of the right tail of a random cost, allowing the designer to strike a balance between the risk-neutral and the worst-case scenario.

While the ability to interpolate between the main paradigms is beneficial, the drawback is the computational burden; the cost functions of multistage RAOCs involve the composition of several nonsmooth risk measures.

Historically, RAOCs were (slowly) solved using stochastic dual dynamic programming (SDDP) [13], [14] approaches such as [15], [16]. The modern approach [17] reformulates RAOCs to allow their solution through popular optimization software such as MOSEK [18], GUROBI [19], and IPOPT [20]. The shortcomings of these interior-point solvers [21] include scalability with the problem size and significant memory requirements.

Despite the recent boom in GPU hardware and software, GPUs are mostly neglected in optimal control problems. Successful examples in stochastic control are [22], [23].

To address these issues, the SPOCK algorithm [24, Algo. 3] was recently proposed; this is a massively parallel proximal method for solving RAOCs. The SPOCK algorithm employs the Chambolle-Pock (CP) method [25] accelerated by the SuperMann framework [26] with Anderson’s acceleration (AA) [27]. This allows the combination of the parallelisable nature of CP with the fast convergence properties

*This paper has received funding by the project “Bot-Dozer: GPU-accelerated model predictive control for autonomous heavy equipment,” which is part of the Doctoral Training Grant No S3809ASA, funded by EPSRC.

[†]Queen’s University Belfast, School of EECS, i-AMS Centre, Ashby Building, BT9 5AH, Belfast, UK

of SuperMann. Earlier, a serial implementation of SPOCK in Julia [28] was tested, and while the results were promising, the serial implementation ignored the rich structure of RAOCPs, leading to limited scalability. Here we propose a GPU-accelerated implementation of SPOCK, which exhibits high scalability, low solve times, and a low memory footprint.

The CP method was selected for its simple, gradient-free iterates. While the CP method is similar to the celebrated alternating direction method of multipliers (ADMM) [25, Sec. 4.3], ADMM requires an extra invocation of a computationally expensive linear operator. Indeed, our results found that the CP method outperforms ADMM for RAOCPs.

The main contributions of this paper are:

1. a novel solver that does not suffer from the scalability issues of interior-point solvers,
2. we demonstrate via extensive benchmarking that SPOCK is amenable to parallelism on a GPU and compare its performance against state-of-the-art solvers in terms of computation time and memory usage,
3. we propose a simple preconditioning of the problem data that leads to improved convergence properties, and
4. we investigate the effect of the scenario tree structure on parallelizability, and so on solve time.

The novel solver, GPU-accelerated SPOCK, paves the way for real-time optimal control in high-dimensional and uncertain environments, offering a promising avenue for both academic research and practical applications.

2 Notation

Let $\mathbb{N}_{[k_1, k_2]}$ denote the integers in $[k_1, k_2]$, let 1_n and 0_n refer to n -dimensional column vectors of ones and zeroes respectively, and let I_n be understood as the n -dimensional identity matrix. We denote n -dimensional positive semidefinite and positive definite matrices by \mathbb{S}_+^n and \mathbb{S}_{++}^n respectively. We denote the transpose of a matrix A by A^\top . For $z \in \mathbb{R}^n$ let $[z]_+ = \mathbf{max}\{0, z\}$, where the max is taken element-wise. The adjoint of a linear operator $L : \mathbb{R}^n \rightarrow \mathbb{R}^m$ is the operator $L^* : \mathbb{R}^m \rightarrow \mathbb{R}^n$

that satisfies $y^\top Lx = x^\top L^*y$ for all $x \in \mathbb{R}^n, y \in \mathbb{R}^m$. The set of fixed points of an operator $T : \mathbb{R}^n \rightarrow \mathbb{R}^n$ is denoted $\mathbf{fix} T = \{v \in \mathbb{R}^n \mid v = T(v)\}$. For two linear maps $F_1 : \mathbb{R}^n \rightarrow \mathbb{R}^{m_1}$ and $F_2 : \mathbb{R}^n \rightarrow \mathbb{R}^{m_2}$ we define $F_1 \times F_2 : \mathbb{R}^n \rightarrow \mathbb{R}^{m_1} \times \mathbb{R}^{m_2}$ to be $(F_1 \times F_2)(x) = (F_1(x), F_2(x))$. For linear maps $F_i : \mathbb{R}^n \rightarrow \mathbb{R}^{m_i}$, $i \in \mathbb{N}_{[1, K]}$, we denote $\times_i F_i = F_1 \times \dots \times F_K$. For two linear maps $F_1 : \mathbb{R}^{n_1} \rightarrow \mathbb{R}^{m_1}$ and $F_2 : \mathbb{R}^{n_2} \rightarrow \mathbb{R}^{m_2}$, we define their direct sum as $F_1 \oplus F_2 \ni \mathbb{R}^{n_1+n_2} \ni (x_1, x_2) \mapsto (F_1(x_1), F_2(x_2)) \in \mathbb{R}^{m_1+m_2}$. The dual cone \mathcal{K}^* of a closed convex cone $\mathcal{K} \subseteq \mathbb{R}^n$ is the set $\mathcal{K}^* = \{y \in \mathbb{R}^n \mid y^\top x \geq 0, \forall x \in \mathcal{K}\}$. The relative interior of a convex set $\mathcal{K} \subseteq \mathbb{R}^n$ is denoted by $\mathbf{ri} \mathcal{K}$. We denote the second order cone of dimension d by SOC_d and a translated second order cone by $\text{SOC}_d + a$ where $a \in \mathbb{R}^d$. The indicator of a convex set \mathcal{K} is defined as $\delta_{\mathcal{K}}(x) = 0$, if $x \in \mathcal{K}$, and $\delta_{\mathcal{K}}(x) = \infty$, otherwise. We define the set of extended reals, $\overline{\mathbb{R}} = \mathbb{R} \cup \{\infty\}$. A function $f : \mathbb{R}^n \rightarrow \overline{\mathbb{R}}$ is called *lower semicontinuous* (lsc) if its sublevel sets, $\{x \mid f(x) \leq \alpha\}$, are closed. The domain of a function $f : \mathbb{R}^n \rightarrow \overline{\mathbb{R}}$ is $\mathbf{dom} f = \{x \mid f(x) < \infty\}$. The subdifferential of a convex function $f : \mathbb{R}^n \rightarrow \overline{\mathbb{R}}$ is $\partial f(x) = \{u \in \mathbb{R}^n \mid \forall y \in \mathbb{R}^n, (y - x)^\top u + f(x) \leq f(y)\}$. The conjugate of a function $f : \mathbb{R}^n \rightarrow \overline{\mathbb{R}}$ is $f^*(y) = \sup_{x \in \mathbb{R}^n} \{y^\top x - f(x)\}$. The proximal operator of a proper lsc convex function $f : \mathbb{R}^n \rightarrow \overline{\mathbb{R}}$ with parameter $\gamma > 0$ is

$$\mathbf{prox}_{\gamma f}(x) = \mathbf{arg} \min_v \left\{ f(v) + \frac{1}{2\gamma} \|v - x\|_2^2 \right\}. \quad (1)$$

Where inequality signs are used with vectors (e.g., $x \leq y$, $x, y \in \mathbb{R}^n$), they are understood to hold element-wise. Throughout, the notation superscript i denotes scenario tree nodes, superscript (k) denotes algorithm iterations, and subscript t denotes time steps.

3 Problem statement

In this section we introduce multistage nested RAOCPs on scenario trees and define the problem statement.

3.1 Dynamical system

We consider the following discrete-time affine dynamical system

$$x_{t+1} = A(w_t)x_t + B(w_t)u_t + c(w_t), \quad (2)$$

for $t \in \mathbb{N}_{[0, N-1]}$, with state variable $x_t \in \mathbb{R}^{n_x}$, control input $u_t \in \mathbb{R}^{n_u}$, and constant $c_t \in \mathbb{R}^{n_u}$. The random disturbance $w_t \in \{1, \dots, n_w\}$ is finite valued; for example, it can be an iid process or a Markov chain.

3.2 Scenario trees

A scenario tree is a representation of the dynamics of the system in Equation (2) over a finite number of stages given that the control actions are determined based on the system states in a causal fashion [29], [30], as depicted in Fig. 1. Each time period is called a *stage*, t , and the number of time periods is called the *horizon*, N . For stopped processes, we denote the *stopping* stage by n_b [31, Sec. 9.8]. Each possible realization of Equation (2) at each stage is called a *node*. We enumerate the nodes of a tree with i , where $i = 0$ is the *root* node which corresponds to the initial state of the system. The nodes at subsequent stages for $t \in \mathbb{N}_{[0, N]}$ are denoted by $\mathbf{nodes}(t)$. Let $\mathbf{nodes}(t_1, t_2) = \cup_{t=t_1}^{t_2} \mathbf{nodes}(t)$, where $0 \leq t_1 \leq t_2 \leq N$. The unique *ancestor* of a node $i \in \mathbf{nodes}(1, N)$ is denoted by $\mathbf{anc}(i)$ and the set of *children* of $i \in \mathbf{nodes}(t)$ for $t \in \mathbb{N}_{[0, N-1]}$ is $\mathbf{ch}(i) \subseteq \mathbf{nodes}(t+1)$. Each node is associated with a probability $\pi^i > 0$ of occurring, where $\sum_{i \in \mathbf{nodes}(t)} \pi^i = 1$ for $t \in \mathbb{N}_{[0, N]}$.

Dynamics. The system dynamics h^i on the scenario tree is described by

$$x^i = A^i x^{i-} + B^i u^{i-} + c^i, \quad (3)$$

where $i \in \mathbf{nodes}(0, N-1)$ and $i_- = \mathbf{anc}(i)$. The state x^0 at the root node is assumed to be known.

Constraints. Here we assume that the states and inputs must satisfy the random convex constraints

$$\Gamma_x^i x^i + \Gamma_u^i u^i \in C^i, \quad (4a)$$

$$\Gamma_N^j x^j \in C_N^j, \quad (4b)$$

for $i \in \mathbf{nodes}(0, N-1)$ and $j \in \mathbf{nodes}(N)$, where C^i and C_N^j are closed convex sets, Γ_x^i and Γ_u^i are the state-input constraint matrices and Γ_N^j is the terminal state constraint matrix.

Quadratic-plus-linear costs. In this paper we consider quadratic-plus-linear cost functions. On the scenario tree, for $i \in \mathbf{nodes}(0, N-1)$ and

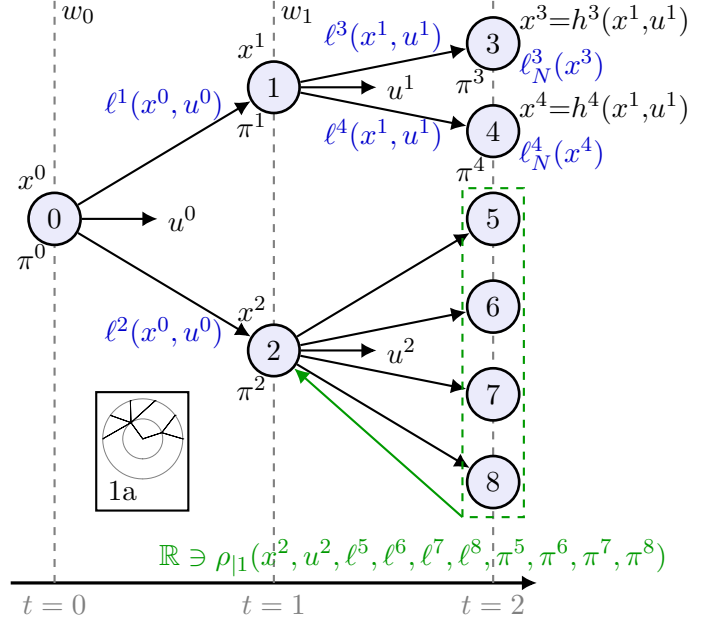


Figure 1: Discrete problem described by a scenario tree. Each node at stage $t+1$ is a possible realization of an event w_t at stage t . The probability of each event is π^i . The dynamics h^i and stage costs ℓ^i are a function of the ancestor state and input, and the event w_t at the ancestor stage t . The terminal costs ℓ_N are a function of the ancestor state and the event w_t at the ancestor stage t . The risk mapping ρ is a many-to-one operator from children to their ancestor. Inset (1a) is a space efficient representation of the tree. The root node at stage 0 is at the center and each consecutive stage is the next concentric circle outwards. This representation will be used later for depicting the branching structure of trees.

$i_- = \text{anc}(i)$, every edge of the tree — that connects the nodes i and i_- — is associated with a stage cost function $\ell^i(x^{i_-}, u^{i_-}) = x^{i_- \top} Q^i x^{i_-} + u^{i_- \top} R^i u^{i_-} + q^{i \top} x^{i_-} + r^{i \top} u^{i_-}$. For $j \in \text{nodes}(N)$, every leaf node is associated with a terminal cost $\ell_N^j(x^j) = x^{j \top} Q_N^j x^j + q_N^{j \top} x^j$.

3.3 Risk measures

Given a discrete sample space $\Omega = \{1, \dots, n\}$ and a probability vector $\pi \in \mathbb{R}^n$, a random cost $Z : \Omega \rightarrow \mathbb{R}$ can be identified by a vector $Z = (Z^1, \dots, Z^n) \in \mathbb{R}^n$. The expectation of Z with respect to π is $\mathbb{E}^\pi[Z] = \pi^\top Z$, and the maximum of Z is defined as $\max Z = \max\{Z^i, i \in \mathbb{N}_{[1,n]}\}$.

A risk measure can be used to reflect the inexact knowledge of the probability measure. A risk measure is an operator, $\rho : \mathbb{R}^n \rightarrow \mathbb{R}$, that maps a random cost $Z \in \mathbb{R}^n$ to a characteristic index $\rho(Z)$ that quantifies the magnitude of its right tail. Coherent risk measures [32, Sec. 6.3] admit the following dual representation

$$\rho(Z) = \max_{\mu \in \mathcal{A}} \mathbb{E}^\mu[Z], \quad (5)$$

where \mathcal{A} is a nonempty closed convex subset of the probability simplex, $\Delta_n := \{\mu \geq 0 : \sum_i \mu_i = 1\}$, known as the *ambiguity set* of ρ . An ambiguity set allows us to quantify the uncertainty in π . This means that coherent risk measures can be seen as a worst-case expectations of Z with respect to a probability vector μ that is taken from \mathcal{A} . The expectation and the maximum can be thought of as the two extreme cases with $\mathcal{A}_{\mathbb{E}} = \{\pi\}$, and $\mathcal{A}_{\max} = \Delta_n$.

Average-value-at-risk. A popular coherent risk measure is the average value-at-risk with parameter $\gamma \in [0, 1]$, denoted by AV@R_γ . It is defined as

$$\text{AV@R}_\gamma[Z] = \begin{cases} \min_{t \in \mathbb{R}^n} \left\{ t + \frac{1}{\gamma} \mathbb{E}^\pi[Z - t]_+ \right\}, & \gamma \neq 0, \\ \max[Z], & \gamma = 0. \end{cases} \quad (6)$$

The ambiguity set of AV@R_γ is

$$\mathcal{A}_\gamma^{\text{avar}}(\pi) = \left\{ \mu \in \mathbb{R}^n \left| \sum_{i=1}^n \mu^i = 1, 0 \leq \mu^i \leq \frac{\pi^i}{\gamma} \right. \right\}. \quad (7)$$

Figure 2 illustrates how AV@R_γ is an interpolation between the risk-neutral ($\text{AV@R}_1 = \mathbb{E}$) and worst-case ($\text{AV@R}_0 = \max$) approaches.

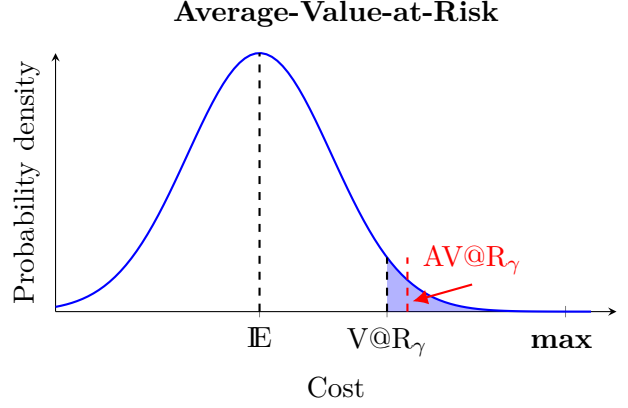


Figure 2: The value-at-risk at level γ of a continuously distributed random cost Z , denoted $V@R_\gamma[Z]$, is the lowest cost x such that $P[Z \geq x] = \gamma$. The average-value at risk at level γ , $\text{AV@R}_\gamma[Z]$, is the expectation of the tail of Z that lies above $V@R_\gamma[Z]$ [33] (shaded area).

Conic representation. Coherent risk measures admit the following conic representation [17]

$$\rho[Z] = \max_{\mu \in \mathbb{R}^n, \nu \in \mathbb{R}^{n_\nu}} \{ \mu^\top Z \mid b - E\mu - F\nu \in \mathcal{K} \}, \quad (8)$$

where \mathcal{K} is a closed convex cone. Provided strong duality holds (i.e., if there exist μ and ν so $b - E\mu - F\nu \in \text{ri}(\mathcal{K})$), the dual form of the risk measure in Equation (8) is

$$\rho[Z] = \min_y \{ y^\top b \mid E^\top y = Z, F^\top y = 0, y \in \mathcal{K}^* \}. \quad (9)$$

For AV@R_γ , $n_\nu = 0$, $b = [\pi^\top \ 0_n^\top \ 1]^\top$, $E = [aI_n \ -I_n \ 1_n]^\top$, and $\mathcal{K} = \mathbb{R}_+^{2n} \times \{0\}$.

3.4 Conditional risk mappings

Let $Z^i = \ell^i(x^{i_-}, u^{i_-})$ and $Z^j = \ell^j(x^j)$ for $i \in \text{nodes}(1, N)$, $j \in \text{nodes}(N)$, and $i_- = \text{anc}(i)$. We define a random variable $Z_t = (Z^i)_{i \in \text{nodes}(t+1)}$ on the probability space $\text{nodes}(t+1)$, for $t \in \mathbb{N}_{[0, N-1]}$. We define a random variable $Z_N = (Z^j)_{j \in \text{nodes}(N)}$ on the probability space $\text{nodes}(N)$.

We define $Z^{[i]} = (Z^{i_+})_{i_+ \in \text{ch}(i)}$, $i \in \text{nodes}(0, N-1)$. This partitions the variable $Z_t = (Z^i)_{i \in \text{nodes}(t)}$ into groups of nodes which share a common ancestor.

Let $\rho : \mathbb{R}^{|\text{ch}(i)|} \rightarrow \mathbb{R}$ be risk measures on the probability space $\text{ch}(i)$. For every stage $t \in \mathbb{N}_{[0, N-1]}$ we may define a conditional risk mapping at stage t , $\rho_t : \mathbb{R}^{|\text{nodes}(t+1)|} \rightarrow \mathbb{R}^{|\text{nodes}(t)|}$, as fol-

lows [32, Sec. 6.8.2]

$$\rho_{|t}[Z_t] = \left(\rho^i[Z^{[i]}] \right)_{i \in \mathbf{nodes}(t)}. \quad (10)$$

3.5 Original problem

An RAOCP with horizon N is defined via the following multistage nested formulation [32, Sec. 6.8.1]

$$V^* = \inf_{u_0} \rho_{|0} \left[Z_0 + \inf_{u_1} \rho_{|1} \left[Z_1 + \dots + \inf_{u_{N-1}} \rho_{|N-1} [Z_{N-1} + Z_N] \dots \right] \right], \quad (11)$$

subject to (3) and (4). Note that the infima in (11) are taken element-wise and with respect to the control laws $u_t = (u^i)_{i \in \mathbf{nodes}(t)}$ for $t \in \mathbb{N}_{[0, N-1]}$. This problem is decomposed using *risk-infimum interchangeability* and *epigraphical relaxation* in [17], allowing us to cast the original problem as the following minimization problem with conic constraints [24]

$$\begin{aligned} & \text{minimize} && s^0 \\ & (x^i)_{i, (x^j)_j, (u^i)_{i, (y^i)_i,} \\ & (\tau^{i+})_{i+, (s^i)_{i, (s^j)_j} \end{aligned} \quad (12a)$$

$$\text{subject to } x^0 = x, \quad (12b)$$

$$x^i = A^i x^{i-} + B^i u^{i-} + c^i, \quad (12c)$$

$$y^i \succ (\kappa^i)^* 0, y^{i\top} b^i \leq s^i, \quad (12d)$$

$$E^{i\top} y^i = \tau^{[i]} + s^{[i]}, F^{i\top} y^i = 0, \quad (12e)$$

$$\ell^i(x^{i-}, u^{i-}) \leq \tau^i, \ell_N^j(x^j) \leq s^j, \quad (12f)$$

$$\Gamma_x^i x^i + \Gamma_u^i u^i \in C^i, \Gamma_N^j x^j \in C_N^j, \quad (12g)$$

for $t \in \mathbb{N}_{[0, N-1]}$, $i \in \mathbf{nodes}(t)$, $i_+ \in \mathbf{ch}(i)$, $i_- = \mathbf{anc}(i)$, and $j \in \mathbf{nodes}(N)$, where $(\cdot)^{[i]} = ((\cdot)^{i+})_{i_+ \in \mathbf{ch}(i)}$, τ and s are slack variables, and x is the initial state.

4 Reformulation

4.1 The Chambolle-Pock method

We can use the CP method to solve optimization problems of the following form [34, p. 32]

$$\mathbb{P} : \text{minimize}_{z \in \mathbb{R}^{n_z}} f(z) + g(Lz), \quad (13)$$

where $L : \mathbb{R}^{n_z} \rightarrow \mathbb{R}^{n_\eta}$ is a linear operator, and f and g are proper closed convex functions on \mathbb{R}^{n_z}

and \mathbb{R}^{n_η} , respectively. We assume strong duality, that is, $\mathbf{ri dom} f \cap \mathbf{ri dom} g(L) \neq \emptyset$, throughout this work.

The CP method [25] recursively applies the firmly nonexpansive (FNE) operator T , where $(z^{(k+1)}, \eta^{(k+1)}) = T(z^{(k)}, \eta^{(k)})$, that is,

$$\begin{aligned} \begin{bmatrix} z^{(k+1)} \\ \eta^{(k+1)} \end{bmatrix} &= \underbrace{\begin{bmatrix} \mathbf{prox}_{\alpha f}(z^{(k)} - \alpha L^* \eta^{(k)}) \\ \mathbf{prox}_{\alpha g^*}(\eta^{(k)} + \alpha L(2z^{(k+1)} - z^{(k)})) \end{bmatrix}}_{T(z^{(k)}, \eta^{(k)})}, \end{aligned} \quad (14)$$

which is a generalized proximal point method with preconditioning operator

$$M(z, \eta) = \begin{bmatrix} I & -\alpha L^* \\ -\alpha L & I \end{bmatrix} \begin{bmatrix} z \\ \eta \end{bmatrix}. \quad (15)$$

The CP method will converge to a solution, provided one exists and $0 < \alpha \|L\| < 1$, where the operator norm is $\|L\| = \max \{\|Lz\| : z \in \mathbb{R}^{n_z}, \|z\| \leq 1\}$.

4.2 Epigraphical relaxation of stage costs

In this section we show that the epigraphical relaxation of the stage costs in (12f) can be reformulated as second order conic (SOC) constraints. The following proposition covers the common case where ℓ is a convex quadratic-plus-linear function.

Proposition 1 *Let $Q \in \mathbb{S}_+^n$ with $\mathbf{rank} Q = p \leq n$, $q \in \mathbb{R}^n$ and define the function $\ell(z) = z^\top Q z + q^\top z$. Let $S \in \mathbb{R}^{n \times p}$ be such that $(\ker Q)^\perp = \text{range } S$, so every $z \in \mathbb{R}^n$ can be written uniquely as $z = z' + Se$, with $n \in \ker Q$ and $e \in \mathbb{R}^p$. Define $\tilde{Q} = S^\top Q S$. Then, $(z, \tau) \in \mathbf{epi} \ell$ if and only if*

$$\mathcal{G}_{S, Q, q}(e, z', \tau) \in \text{SOC}_{p+2} + a_{S, Q, q}, \quad (16)$$

where $\mathcal{G}_{S, Q, q}$ is the linear map

$$\mathcal{G}_{S, Q, q}(e, z', \tau) = \begin{bmatrix} \tilde{Q}^{1/2} e \\ \frac{1}{2} \tau - \frac{1}{2} q^\top z' \\ \frac{1}{2} \tau - \frac{1}{2} q^\top z' \end{bmatrix}, \quad (17a)$$

and

$$a_{Q, q} = \begin{bmatrix} -\frac{1}{2} \tilde{Q}^{-1/2} S^\top q \\ -\frac{1}{8} \|S^\top q\|_{\tilde{Q}^{-1}}^2 + \frac{1}{2} \\ -\frac{1}{8} \|S^\top q\|_{\tilde{Q}^{-1}}^2 - \frac{1}{2} \end{bmatrix}. \quad (17b)$$

If $Q \in \mathbb{S}_{++}$, then $S = I$ and $\tilde{Q} = Q$; in this case we will be using the notation $\mathcal{G}_{Q, q} = \mathcal{G}_{I, \tilde{Q}, q}$ and $a_{Q, q} = a_{I, \tilde{Q}, q}$.

Proof. We have $\ell(z) = z^\top Qz + q^\top z = r^\top \tilde{Q}r + q^\top Se + q^\top z'$. By completing the squares we have $\ell = \|e + \frac{1}{2}\tilde{Q}^{-1}S^\top q\|_{\tilde{Q}}^2 - \frac{1}{4}\|S^\top q\|_{\tilde{Q}^{-1}}^2$, therefore, $(z, \tau) \in \mathbf{epi} \ell$ if and only if

$$\begin{aligned} \|e + \frac{1}{2}\tilde{Q}^{-1}S^\top q\|_{\tilde{Q}}^2 &\leq \tau + \frac{1}{4}\|S^\top q\|_{\tilde{Q}^{-1}}^2 \\ \Leftrightarrow \|\tilde{Q}^{1/2}e + \frac{1}{2}\tilde{Q}^{-1/2}S^\top q\|_2^2 &\leq \tau + \frac{1}{4}\|S^\top q\|_{\tilde{Q}^{-1}}^2, \end{aligned} \quad (18)$$

and using the identity $\tau = (\frac{\tau+1}{2})^2 - (\frac{\tau-1}{2})^2$ we can show that this is equivalent to the condition of Equation (16). \square

In some applications it is expedient to include an ℓ_1 -type of penalty in the stage cost to enforce sparseness.

Proposition 2 *Let $Q \in \mathbb{S}_{++}^n$, $q \in \mathbb{R}^n$, $\lambda_0 > 0$, and define the function $\ell(z) = z^\top Qz + q^\top z + \lambda_0\|z\|_1$. Then $(z, \tau) \in \mathbf{epi} \ell$ if and only if there exists scalars $\theta \in \mathbb{R}$ and $\lambda_1, \dots, \lambda_n \geq 0$ such that*

$$\mathcal{G}_{Q,q}(e, z', \tau - \lambda_0\theta) \in \text{SOC}_{p+2} + a_{Q,q}, \quad (19)$$

and $\sum_{i=1}^n \lambda_i \leq \theta$ and $-\lambda_i \leq z_i \leq \lambda_i$ for $i = 1, \dots, n$.

Proof. We have that $z^\top Qz + q^\top z + \lambda_0\|z\|_1 \leq \tau$ is equivalent to the existence of a $\theta \in \mathbb{R}$ such that

$$z^\top Qz + q^\top z + \lambda_0\theta \leq \tau, \quad (20a)$$

$$\|z\|_1 \leq \theta, \quad (20b)$$

where, by Proposition 1, the first condition yields Equation (19). The second condition is equivalent to $\sum_{i=1}^n |z_i| \leq \theta$ and using the relaxation $|z_i| \leq \theta$ completes the proof. \square

Following the same approach we can accommodate stage cost functions that involve soft constraints with quadratic penalty functions, e.g., functions of the form $\ell(z) = z^\top Qz + q^\top z + \|\mathbf{max}(0, z - z_{\max})\|^2$, with $Q \in \mathbb{S}_+^n$, where the maximum is meant in the element-wise sense. The constraint $\ell(z) \leq \tau$ can be written as

$$\begin{bmatrix} z \\ \theta \end{bmatrix}^\top \begin{bmatrix} Q & \\ & 1 \end{bmatrix} \begin{bmatrix} z \\ \theta \end{bmatrix} + \begin{bmatrix} q \\ 0 \end{bmatrix}^\top \begin{bmatrix} z \\ \theta \end{bmatrix} \leq \tau, \quad (21)$$

with $\theta \geq 0$ and $x - x_{\max} \leq \theta$, and Equation (21) can be handled using Proposition 1.

4.3 Sets

Define $z = (s^0, z_1, z_2)$, where $z_1 = ((x^{i'})_{i'}, (u^i)_i)$, and $z_2 = (y^i, \tau^{[i]}, s^{[i]})$, for $i' \in \mathbf{nodes}(0, N)$ and $i \in \mathbf{nodes}(0, N-1)$. We define the sets

$$\mathcal{S}_1 = \left\{ z_1 \left| \begin{array}{l} x^0 - x = 0, \\ x^i - A^i x^{i-} - B^i u^{i-} - c^i = 0, \\ \forall i \in \mathbf{nodes}(1, N), i_- = \mathbf{anc}(i). \end{array} \right. \right\}, \quad (22)$$

$$\mathcal{S}_2 = \prod_{i \in \mathbf{nodes}(0, N-1)} \ker \underbrace{\begin{bmatrix} E^{i\top} & -I & -I \\ F^{i\top} & 0 & 0 \end{bmatrix}}_{S_2^i}, \quad (23)$$

$$\begin{aligned} \mathcal{S}_3 = & \prod_{i \in \mathbf{nodes}(0, N-1)} ((\mathcal{K}^i)^* \times \mathbb{R}_+ \times C^i) \\ & \times \prod_{i \in \mathbf{nodes}(1, N)} (\text{SOC}_{n_x+n_u+2} + a^i) \\ & \times \prod_{j \in \mathbf{nodes}(N)} \left(C^j \times (\text{SOC}_{n_x+2} + a_N^j) \right), \end{aligned} \quad (24)$$

where $a^i = a_{\text{blkdiag}(Q^i, R^i), [q^{i\top} \ r^{i\top}]^\top}$ and $a_N^j = a_{Q_N^j, q_N^j}$.

4.4 Linear operator L

We define the linear operator L that maps z to

$$\begin{aligned} \eta = & ((y^i, s^i - b^{i\top} y^i, \Gamma_x^i x^i + \Gamma_u^i u^i)_{i \in \mathbf{nodes}(0, N-1)}, \\ & ((Q^i)^{1/2} x^{\mathbf{anc}(i)}, (R^i)^{1/2} u^{\mathbf{anc}(i)}, \\ & \quad \frac{1}{2}\tau^i, \frac{1}{2}\tau^i)_{i \in \mathbf{nodes}(1, N)}, \\ & (\Gamma_N^j x^j, ((Q_N^j)^{1/2} x^j, \frac{1}{2}s^j, \frac{1}{2}s^j))_{j \in \mathbf{nodes}(N)}). \end{aligned} \quad (25)$$

It can be seen that there is a permutation $\Pi : \mathbb{R}^{n_z} \rightarrow \mathbb{R}^{n_z}$ such that $L \circ \Pi$ is block-diagonal with

$$L \circ \Pi = \bigoplus_{i \in \mathbf{nodes}(0, N-1)} L_i \oplus \bigoplus_{j \in \mathbf{nodes}(N)} L_N^j \oplus D_0, \quad (26)$$

where

$$D_i = \bigtimes_{i_+ \in \mathbf{ch}(i)} \text{blkdiag}(Q^{i_+}, R^{i_+}, \frac{1}{2}1_2) \quad (27)$$

$$D_N^j = \text{blkdiag}(Q^j, \frac{1}{2}1_2) \quad (28)$$

$$b = \bigtimes_{i \in \mathbf{nodes}(0, N-1)} b^i, \quad (29)$$

$$D_0 = \begin{bmatrix} 1_{n_b}^\top & 0_{|\mathbf{nodes}(0, N-1)|}^\top \\ b^* & 1_{|\mathbf{nodes}(0, N-1)|}^\top \end{bmatrix}, \quad (30)$$

$$L^i = D^i \times [\Gamma_x^i \ \Gamma_u^i \ 0_{n_g \times n_c}], \quad (31)$$

$$L_N^j = D_N^j \times [\Gamma_N^j \ 0_{n_g}]. \quad (32)$$

It follows that

$$\|L\| = \|L \circ \Pi\| = \max \left\{ (\|L_i\|)_i, (\|L_N^j\|)_j, \|D_0\| \right\}. \quad (33)$$

Using the property $\|\times_{i=1}^v L_i\| \leq \sqrt{v} \max_{i=1,\dots,v} \|L_i\|$, it follows that $\|L\|$ is controlled by

$$\max_{i,j} \{ \sqrt{|\text{ch}(i)|} \max(\|Q^{i+}\|, \|R^{i+}\|), \|\Gamma_x^i \Gamma_u^i\|, \|Q^j\|, \|\Gamma_N^j\| \} \quad (34)$$

In other words, $\|L\|$ —and, importantly, the CP step size α —scales with the largest number of children per node, not the prediction horizon N .

4.5 Operator splitting

We can now write Problem (12) as

$$\underset{z}{\text{minimize}} \quad s^0 \quad (35a)$$

$$\text{subject to } z_1 \in \mathcal{S}_1, z_2 \in \mathcal{S}_2, \eta \in \mathcal{S}_3, \quad (35b)$$

which is equivalent to (13)

$$\underset{z}{\text{minimize}} \quad f(z) + g(Lz), \quad (36)$$

where

$$f(z) = s^0 + \delta_{\mathcal{S}_1}(z_1) + \delta_{\mathcal{S}_2}(z_2), \quad (37a)$$

$$g(\eta) = \delta_{\mathcal{S}_3}(\eta). \quad (37b)$$

5 Numerical algorithm

5.1 Proximal operators

The proximal operators in (14) remain largely the same as in [24], however, here we extend the projection on the dynamics to allow the affine set \mathcal{S}_1 . We denote the primal vector before projection by \bar{z} . Computing $\text{proj}_{\mathcal{S}_1}(\bar{z}_1)$ comprises the offline Algorithm 1 from [24], which we show here for completeness, and the online Algorithm 2. Algorithm 1 is run offline once, and Algorithm 2 is run online once per projection on \mathcal{S}_1 .

5.2 SPOCK algorithm

We state the parallelized SPOCK algorithm from [24, Algo. 3]. We define $v = [z^\top \quad \eta^\top]^\top$. Note that we do not explicitly form or store the matrices L , L^* or M . The SPOCK algorithm follows the SuperMann [26] framework, a Newton-type algorithm that finds a

Algorithm 1 Projection on \mathcal{S}_1 : Offline

Require: Matrices $(A^i)_i$ and $(B^i)_i$, and horizon N
Ensure: Matrices $(K^i)_i$, $(P^i)_i$, $(\tilde{R}^i)_i$ and $(\bar{A}^i)_i$

- 1: **for all** $i \in \text{nodes}(N)$ **in parallel do**
- 2: $P^i \leftarrow I_{n_x}$
- 3: **for** $t = 0, 1, \dots, N - 1$ **do**
- 4: **for all** $i \in \text{nodes}(N - (t + 1))$ **in parallel do**
- 5: $\tilde{P}^{i+} \leftarrow B^{i+\top} P^{i+}$, $i_+ \in \text{ch}(i)$
- 6: $\tilde{R}^i \leftarrow I_{n_u} + \sum_{i_+ \in \text{ch}(i)} \tilde{P}^{i+} B^{i+}$ and determine its Cholesky decomposition
- 7: $K^i \leftarrow -(\tilde{R}^i)^{-1} \sum_{i_+ \in \text{ch}(i)} \tilde{P}^{i+} A^{i+}$
- 8: $\bar{A}^{i+} \leftarrow A^{i+} + B^{i+} K^i$, $i_+ \in \text{ch}(i)$
- 9: $P^i \leftarrow I_{n_x} + K^{i\top} K^i + \sum_{i_+ \in \text{ch}(i)} \bar{A}^{i+\top} P^{i+} \bar{A}^{i+}$

Algorithm 2 Projection on \mathcal{S}_1 : Online

Require: Matrices computed by Algorithm 1, constants $(c^i)_i$, vector \bar{z}_1 as defined in Sec. 4.5, and initial state x^0
Ensure: Projection on \mathcal{S}_1 at \bar{z}_1

- 1: **for all** $i \in \text{nodes}(N)$ **in parallel do**
- 2: $q_0^i \leftarrow -\bar{x}^i$
- 3: **for** $t = 0, 1, \dots, N - 1$ **do**
- 4: **for all** $i \in \text{nodes}(N - (t + 1))$ **in parallel do**
- 5: $\bar{d}^i \leftarrow \sum_{i_+ \in \text{ch}(i)} B^{i+\top} (q^{i+} + P^{i+} c^{i+})$
- 6: $d_{t+1}^i \leftarrow (\tilde{R}^i)^{-1} (\bar{u}^i - \bar{d}^i)$ using Cholesky of \tilde{R}^i
- 7: $\bar{q}^i \leftarrow \sum_{i_+ \in \text{ch}(i)} \bar{A}^{i+\top} (P^{i+} (B^{i+} d^i + c^{i+}) + q^{i+})$
- 8: $q_{t+1}^i \leftarrow K^{i\top} (d^i - \bar{u}^i) - \bar{x}^i + \bar{q}^i$
- 9: $x^0 \leftarrow x$
- 10: **for** $t = 0, 1, \dots, N - 1$ **do**
- 11: **for all** $i \in \text{nodes}(t)$, $i_+ \in \text{ch}(i)$ **in parallel do**
- 12: $u^i \leftarrow K^i x^i + d^i$
- 13: $x^{i+} \leftarrow A^{i+} x^i + B^{i+} u^i + c^{i+}$
- 14: **return** $z_1 \leftarrow \text{proj}_{\mathcal{S}_1}(\bar{z}_1)$.

fixed point of firmly nonexpansive operators. The framework involves two extragradient-type updates that can involve fast (e.g., quasi-Newtonian) directions to enjoy the same global convergence properties as the classical Krasnosel'skiĭ-Mann scheme.

These directions are computed using Anderson's acceleration [27] as described in Algorithm 3, and is discussed further in Section 6.2 along with the choice of parameter m . AA uses two matrices, $M_r, M_d \in \mathbb{R}^{n_v \times m}$, to keep a running store of the last m residuals and their differences, respectively.

Algorithm 3 Anderson's acceleration

Require: Memory length m , residual $r^{(k)}$, and matrices M_r and M_d .
Ensure: Fast direction $\psi^{(k)}$ and matrices M_r and M_d

- 1: Shift columns of M_r and M_d to the right by 1
- 2: $M_r(:, 0) \leftarrow r^{(k)}$
- 3: $M_d(:, 0) \leftarrow M_r(:, 0) - M_r(:, 1)$
- 4: **if** $k \leq m$ **then**
- 5: $\psi^{(k)} \leftarrow -r^{(k)}$ **return** $\psi^{(k)}$
- 6: **if** columns of M_r and M_d are greater than m **then**
- 7: Delete last column of M_r and M_d
- 8: $Q^{(k)}, R^{(k)} \leftarrow M_d$ by QR decomposition
- 9: Solve $R^{(k)}\kappa = Q^{(k)\top}r^{(k)}$ for κ
- 10: $\psi^{(k)} \leftarrow -r^{(k)} - (M_r - M_d)\kappa$
- 11: **return** $\psi^{(k)}$

For the other SPOCK parameters, we refer to [26, Sec. VI.D], that is, set $c_0 = 0.99$, $c_1 = 0.99$, $c_2 = 0.99$, $\beta = 0.5$, $\sigma = 0.1$, and $\lambda = 1$. Indeed, these values have shown to be effective after some parameter testing.

5.3 Termination conditions

We define the residual operator $R = \text{id} - T$, where id is the identity operator. The SuperMann algorithm finds a fixed point $v^* \in \text{fix } T$ of a firmly nonexpansive operator T by finding a zero of R . Therefore, it makes sense to terminate SPOCK when $\|R^{(k)}\|_\infty \leq \max(\epsilon_{\text{abs}}, \epsilon_{\text{rel}}\|R^{(0)}\|_\infty)$ for some small $0 < \epsilon_{\text{abs}}, \epsilon_{\text{rel}} \in \mathbb{R}$. However, this does not guarantee v^* is an ϵ -approximate optimal point to \mathbb{P} , as we now discuss.

The optimality condition for \mathbb{P} is $0 \in \partial f(z) +$

Algorithm 4 SPOCK algorithm for RAOCPs

Require: problem data, $z^{(0)}$ and $\eta^{(0)}$, tolerances $\epsilon_{\text{abs}} > 0$ and $\epsilon_{\text{rel}} > 0$, α such that $0 < \alpha\|L\| < 1$, $\mathbb{N} \ni m > 0$, $c_0, c_1, c_2 \in [0, 1)$, $\beta, \sigma \in (0, 1)$, and $\lambda \in (0, 2)$.

Ensure: approximate solution of RAOCP

- 1: Compute offline matrices via Algorithm 1
- 2: $r^{(0)} \leftarrow v^{(0)} - T(v^{(0)})$, $\zeta_{(0)} \leftarrow \|r^{(0)}\|_M$
- 3: $\omega_{\text{safe}} \leftarrow \zeta_{(0)}$, $k \leftarrow 0$
- 4: **if** termination criteria (Sec. 5.3) are satisfied **then**
- 5: **return** $v^{(k)}$
- 6: $r^{(k)} \leftarrow v^{(k)} - T(v^{(k)})$
- 7: $\psi^{(k)} \leftarrow$ Algorithm 3
- 8: $\omega_{(k)} \leftarrow \|r^{(k)}\|_M$
- 9: **if** $\omega_{(k)} \leq c_0\zeta_{(k)}$ **then**
- 10: $v^{(k+1)} \leftarrow v^{(k)} + \psi^{(k)}$, (K0)
- 11: $\zeta_{(k+1)} \leftarrow \omega_{(k)}$, **goto** line 20
- 12: $\zeta_{(k+1)} \leftarrow \zeta_{(k)}$, $\tau \leftarrow 1$
- 13: $\tilde{v}^{(k)} \leftarrow v^{(k)} + \tau\psi^{(k)}$, $\tilde{r}^{(k)} \leftarrow \tilde{v}^{(k)} - T(\tilde{v}^{(k)})$
- 14: $\tilde{\omega}_{(k)} \leftarrow \|\tilde{r}^{(k)}\|_M$
- 15: **if** $\omega_{(k)} \leq \omega_{\text{safe}}$ **and** $\tilde{\omega}_{(k)} \leq c_1\omega_{(k)}$ **then**
- 16: $v^{(k+1)} \leftarrow \tilde{v}^{(k)}$, (K1)
- 17: $\omega_{\text{safe}} \leftarrow \tilde{\omega}_{(k)} + c_2^k$, **goto** line 20
- 18: $\rho_{(k)} \leftarrow \tilde{\omega}_{(k)}^2 - 2\alpha(\tilde{r}^{(k)})^\top M(\tilde{v}^{(k)} - v^{(k)})$
- 19: **if** $\rho_{(k)} \geq \sigma\tilde{\omega}_{(k)}\omega_{(k)}$ **then**
- 20: $v^{(k+1)} \leftarrow v^{(k)} - \frac{\lambda\rho_{(k)}}{\tilde{\omega}_{(k)}^2}\tilde{r}^{(k)}$ (K2)
- 21: **else** $\tau \leftarrow \beta\tau$, **goto** line 12
- 22: $k \leftarrow k + 1$, **goto** line 4

$L^* \partial g(Lz)$ assuming $\mathbf{ri dom} f \cap \mathbf{ri dom} g(L) \neq \emptyset$, or

$$0 \in \partial f(z) + L^* \eta, \quad (38a)$$

$$0 \in \partial g^*(\eta) - Lz, \quad (38b)$$

for some $z \in \mathbb{R}^n$ and $\eta \in \mathbb{R}^m$.

To define a notion of approximate optimality, we firstly introduce a notion of ϵ -approximate belonging to a set. For a set $\mathcal{X} \subseteq \mathbb{R}^n$, the notation $x \in_\epsilon \mathcal{X}$ means that there is a $\xi \in \mathbb{R}^n$, with $\|\xi\|_\infty \leq \epsilon$ and $x + \xi \in \mathcal{X}$.

Definition 3 (Approximate optimality) A point $(\tilde{z}, \tilde{\eta})$ is said to be an ϵ -approximate primal-dual optimal point for \mathbb{P} if $0 \in_\epsilon \partial f(\tilde{z}) + L^* \tilde{\eta}$ (primal condition) and $0 \in_\epsilon \partial g^*(\tilde{\eta}) - L\tilde{z}$ (dual condition).

Next, we turn our attention to the CP operator to determine appropriate primal and dual residuals. The primal update in (14) can be written as

$$\begin{aligned} \alpha \partial f(z^{(k+1)}) + z^{k+1} &\ni z^{(k)} - \alpha L^* \eta^{(k)} \\ \Leftrightarrow \underbrace{\frac{\Delta z^k}{\alpha} - L^*(\Delta \eta^k)}_{\xi_1^{(k)}} &\in L^* \eta^{(k+1)} + \partial f(z^{(k+1)}), \end{aligned} \quad (39)$$

with $\Delta z^{(k)} = z^{(k)} - z^{(k+1)}$ and $\Delta \eta^{(k)} = \eta^{(k)} - \eta^{(k+1)}$. We, therefore, define the residual $\xi_1^{(k)}$ as in Equation (39). Likewise, we define the residual $\xi_2^{(k)}$

$$\begin{aligned} \alpha \partial g^*(\eta^{(k+1)}) + \eta^{(k+1)} - 2\alpha Lz^{(k+1)} &\ni \eta^k - \alpha Lz^{(k)} \\ \Leftrightarrow \underbrace{\frac{\Delta \eta^k}{\alpha} - L(\Delta z^{(k)})}_{\xi_2^{(k)}} &\in \partial g^*(\eta^{(k+1)}) - Lz^{(k+1)}. \end{aligned} \quad (40)$$

If $\|\xi_1^{(k+1)}\|_\infty \leq \epsilon$, and $\|\xi_2^{(k+1)}\|_\infty \leq \epsilon$, then $(z^{(k+1)}, \eta^{(k+1)})$ is an ϵ -approximate optimal point.

Remark: suppose $(z^{(k+1)}, \eta^{(k+1)})$ is an ϵ -approximate optimal point. Then, $Lz^{(k+1)} \in_\epsilon \partial g^*(\eta^{(k+1)})$. Let (z^*, η^*) be a fixed point of the CP method. Then, $Lz^* \in \partial g^*(\eta^*)$. If ∂g^* is metrically regular with modulus τ at (η^*, Lz^*) [35, Sect. 9.G], then $\eta^{(k+1)} \in_{\epsilon\tau} \partial g(Lz^{(k+1)})$. As a result, $0 \in_{\epsilon'} \partial f(z^{(k+1)}) + L^* \partial g(Lz^{(k+1)})$ with $\epsilon' = \epsilon(1 + \tau\|L^*\|_\infty)$, i.e., the pair $(z^{(k+1)}, \eta^{(k+1)})$ satisfies approximately the original optimality conditions.

5.4 Preconditioning

Both CP and SPOCK are first-order methods, so they can benefit from preconditioning. It is possible to precondition the CP method at the expense of a higher per-iteration computation cost [36]. Here,

however, we use heuristic preconditioning matrices to scale the problem — that is, increase the step size — offline. In Section 4.4, we see that the step size of the CP method is proportional to $\|L\|$, and so to the cost matrices Q and R . As a result, we scale the states and inputs by the diagonal matrices $S^x \in \mathbb{S}_{++}^{n_x}$ and $S^u \in \mathbb{S}_{++}^{n_u}$ respectively, where

$$\hat{c} = \sqrt{\max(|\mathbf{ch}(i)|)} \quad (41a)$$

$$S_{kk}^x = \hat{c} \max \left\{ 1, ((Q_{kk}^i)^{1/2})_i \right\}, \quad (41b)$$

$$S_{kk}^u = \hat{c} \max \left\{ 1, ((R_{kk}^i)^{1/2})_i \right\}, \quad (41c)$$

$$S_{N,kk}^x = \max \left\{ 1, ((Q_{N,kk}^j)^{1/2})_j \right\}, \quad (41d)$$

for $i \in \mathbf{nodes}(1, N)$ and $j \in \mathbf{nodes}(N)$. In other words, we introduce a change of variables $\tilde{x}^i = S^x x^i$, and $\tilde{u}^i = S^u u^i$ for $i \in \mathbf{nodes}(1, N-1)$, and $\tilde{x}^j = S_N^x x^j$, $j \in \mathbf{nodes}(1, N)$. Alongside, the tolerance in the termination criteria is scaled accordingly. The constraints become $\Gamma_x^i S_x^{-1} \tilde{x}^i + \Gamma_u^i S_u^{-1} \tilde{u}^i \in C^i$ and $\Gamma_N^j S_x \tilde{x}^j \in C_N^j$ for $i \in \mathbf{nodes}(0, N-1)$ and $j \in \mathbf{nodes}(N)$. We define $a^i = \max\{1, \|\Gamma_x^i S_x^{-1} \Gamma_u^i S_u^{-1}\|\}$ and scale the constraints as $\frac{1}{a^i} \Gamma_x^i S_x^{-1} \tilde{x}^i + \frac{1}{a^i} \Gamma_u^i S_u^{-1} \tilde{u}^i \in \frac{1}{a^i} C^i$.

This change of variables and rescaling of the constraints is shown to prevent $\|L\|$ from becoming too large and the step size from becoming too small.

6 Parallel computing

There are two important factors, data type and block size, that must be considered when dealing with parallel computing. There is a trade-off between speed and accuracy in data types, that is, using the `float` type will decrease execution time at the cost of accuracy compared to using the `double` type. The block size, or threads per block, is a programming abstraction that determines how many threads are executed in parallel. While choosing the optimal block size is hardware specific, it is recommended to use multiples of the warp size [37] (32 for all current NVIDIA hardware and compute capabilities [38, Tab. 16]) so that warps are fully utilized.

For SPOCK in particular, we recommend the `float` type for solving problems to lax tolerances (10^{-3}), and the `double` type for strict tolerances (10^{-5}). Furthermore, we recommend the block size to be at least the number of states plus the number of inputs plus two, i.e., $n_x + n_u + 2$. This ensures optimal performance of projections on SOCs.

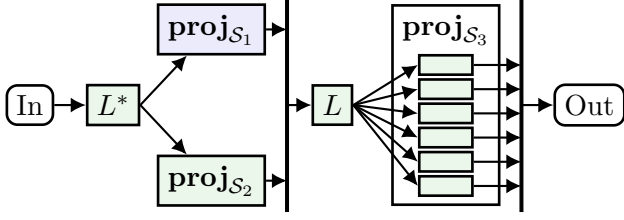


Figure 3: Fork-join chain of streams of main parallelized processes in a CP iteration.

6.1 Tree structure exploitation

In order to extract the most benefit from parallel computing, we must first understand the parallel nature of each process in the solver. Figure 3 illustrates the fork-join chain of the main parallelized processes in a CP iteration. The projection on the dynamics (\mathcal{S}_1) is parallelized per stage. The projections on sets \mathcal{S}_2 and \mathcal{S}_3 , and the operators L and L^* , are all parallelized per node. However, there is serial summations across siblings within the dynamics projection and L^* operator. As such, a tree structure with high initial branching and no further branching will benefit the most from parallelization.

6.2 Anderson’s acceleration

In line 7 of Algorithm 4, we follow the same method as before [24, Sec. 6.2], with memory length $m = 3$, to compute the directions required. Here, however, we use the CUDA libraries cuSOLVER and cuBLAS to compute the least squares solution. In particular, we compute the QR factorization of a tall matrix with `cusolverDn<t>geqrf` that stores the resulting orthogonal matrix Q as a sequence of Householder vectors. Then, we use `cusolverDn<t>ormqr` and `cublas<t>trsm` to solve the triangular linear system. With this approach, we compared longer memory lengths of up to $m = 10$, and found that $m = 3$ performed best in all test cases.

This approach can be improved by initially computing the QR factorization in this way, and then updating the Q and R matrices using Givens rotations [39].

6.3 GPUutils

Much of SPOCK is built on the lightweight GPUutils [40], an open-source header-only library. GPUutils makes managing and manipulating device

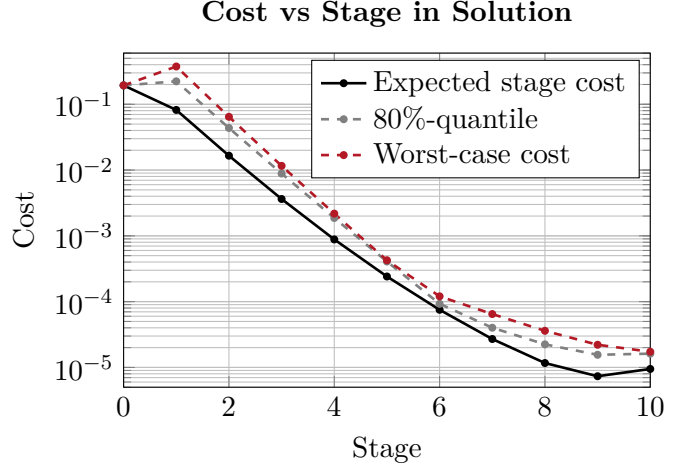


Figure 4: Cost vs Stage plot for an instance of the problem in [24, Sec. 7] with a horizon of 10.

data easy and memory-safe. In particular, this library brings easy C++-type linear algebra operators to CUDA C++.

7 Results

As the CP method shares many similarities with ADMM [25, Sec. 4.3], our first experiment compared the popular ADMM algorithm against the CP method with the same parallelized code, however, this resulted in more iterations, and more computation per iteration, to obtain the same tolerance.

The next experiment gave an insight into the solution returned by the solver. Figure 4 shows the stage-wise distribution of costs for an instance of the problem in [24, Sec. 7], with $n_x, n_u, n_w, N = 10$ and $n_b = 1$. As we expect, the expected cost goes to zero as the stage progresses.

7.1 Speedup compared to serial SPOCK

To evaluate the performance improvement of GPU-accelerated SPOCK, we compare its execution time of the problem in [24, Sec. 7] against the serial implementation for different problem sizes. Figure 5 illustrates the speedup factor, defined as the ratio of the execution time of the serial SPOCK to that of the GPU-accelerated SPOCK.

The GPU-accelerated SPOCK achieves significant speedup across larger problem sizes, both in terms of number of nodes and number of states and inputs. This demonstrates the effectiveness of leveraging parallel computing hardware to handle the

Speedup of parallelisation of SPOCK

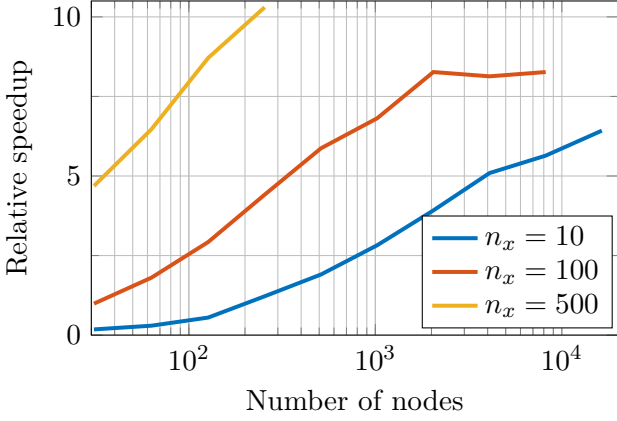


Figure 5: Speedup factor of GPU-accelerated SPOCK compared to serial SPOCK for the problem in [24, Sec. 7], where n_x is the number of states and also the number of inputs, i.e., $n_u = n_x$.

computationally intensive tasks in the SPOCK algorithm.

8 Applications

8.1 Case study 1 (Benchmarks)

To evaluate the solve time of SPOCK, we compare it against the popular solvers MOSEK, GUROBI, and IPOPT for a variety of random problems.

8.1.1 Problem statement

We generated a random collection of (large to very large) risk-averse optimal control problems (cf. Equation (2)) along the lines of [41, Sec. A.3]. We sample prediction horizons $N \sim \mathcal{U}(5, 15)$, and jointly sample n_b , n_w , and n_u from the uniform distribution on the set

$$\left\{ \begin{bmatrix} b \\ w \\ u \end{bmatrix} \in \mathbb{N}^3 \mid \begin{array}{l} 1 \leq b \leq 3, \\ 2 \leq w \leq 10, \\ 10 \leq u \leq 300, \\ 10^3 \leq n_v \leq 10^5 \end{array} \right\},$$

where n_v is the number of variables, i.e., $n_v = n_x \cdot |\text{nodes}(0, N)| + n_u \cdot |\text{nodes}(0, N - 1)|$. We fix $n_x = 2n_u$. We impose box state and input constraints, $-\bar{x} \leq x_{t+1} \leq \bar{x}$, and $-\bar{u} \leq u_t \leq \bar{u}$, for all $t \in \mathbb{N}_{[0, N-1]}$, with $\bar{x} \sim \mathcal{U}([1, 2]^{n_x})$ and $\bar{u} \sim \mathcal{U}([0, 0.1]^{n_u})$. We use AV@R_γ as the risk measure with parameter $\gamma \sim \mathcal{U}([0, 1])$ with a random base probability vector $\pi \sim \mathcal{U}(\Delta_{n_w})$,

where Δ_{n_w} is the probability simplex in \mathbb{R}^{n_w} . Regarding the system dynamics, we take a random matrix $B \in \mathbb{R}^{n_x \times n_u}$ with elements $B_{ij} \sim \mathcal{N}(0, 1)$ and for each event $w \in \mathbb{N}_{[1, n_w]}$ we take random system matrices

$$A(w) = I_{n_x} + A^w, A_{ij}^w \sim \mathcal{N}(0, 0.01), \quad (42a)$$

$$B(w) = B + B^w, B_{ij}^w \sim \mathcal{N}(0, 0.01). \quad (42b)$$

For the stage costs we define

$$Q_0 = \text{diag}(q_0), q_0 \sim \mathcal{U}([0, 0.1]^{n_x}), \quad (42c)$$

$$R_0 = \text{diag}(r_0), r_0 \sim \mathcal{U}([0, 100]^{n_u}), \quad (42d)$$

and for each event $w \in \mathbb{N}_{[1, n_w]}$

$$Q_{ij}^w \sim \mathcal{N}(0, 0.01), \quad (42e)$$

$$Q(w) = (Q_0 + Q^w)(Q_0 + Q^w)^\top, \quad (42f)$$

$$R_{ij}^w \sim \mathcal{N}(0, 0.01), \quad (42g)$$

$$R(w) = (R_0 + R^w)(R_0 + R^w)^\top, \quad (42h)$$

and $Q_N = Q_0$. Lastly, we sample $x \in \mathbb{R}^{n_x}$ with $x_i \sim \mathcal{U}([-0.5\bar{x}_i, 0.5\bar{x}_i])$.

8.1.2 Performance profiles

We use performance profiles [42] to compare the performance of the SPOCK algorithm with state-of-the-art solvers. We define the performance measure to be the solve time. We limit the solve time to 5 min, and we consider exceeding this limit a failure. Failure is given the ratio $r_M = \infty$.

We present the Dolan-Moré plot of the performance profiles in Figure 6. The plot shows the cumulative distribution of the performance ratios for the solvers MOSEK, GUROBI, IPOPT, and GPU-accelerated SPOCK for a set of 100 random problems. The plot shows the percentage of problems solved within a factor τ of the best solver. The best solver is the one with the shortest solve time for each problem. The plot shows that SPOCK outperforms the other solvers in terms of speed (highest probability at $\tau = 0$) and robustness (highest probability at $\tau = r_M$).

8.1.3 Memory management

The peak RAM usage of each solver was recorded while solving the 100 random problems. CPU and GPU memory usage were combined for GPU-accelerated SPOCK, and the others only use CPU memory. The results are presented in Figure 7, illustrating how SPOCK uses significantly less memory

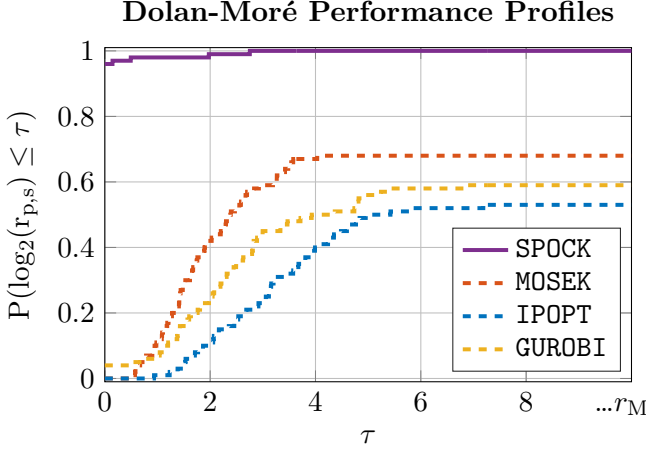


Figure 6: Dolan-Moré plot of popular solvers MOSEK, GUROBI, and IPOPT compared to GPU-accelerated SPOCK for 100 random problems.

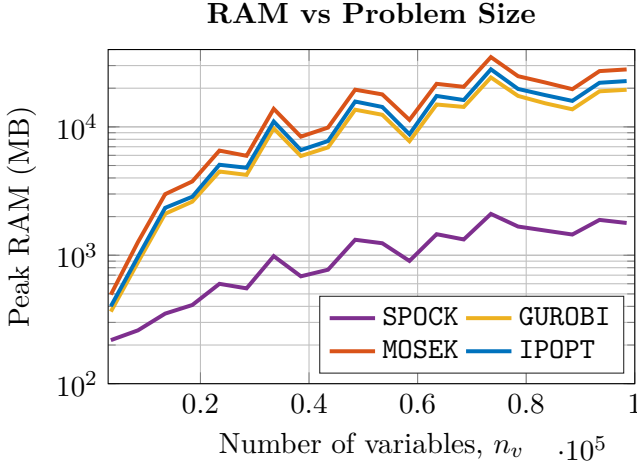


Figure 7: Peak RAM vs problem size of solvers MOSEK, GUROBI, IPOPT, and GPU-accelerated SPOCK for 100 random problems.

than the other solvers. For example, for a problem size of $n_v = 10^5$, SPOCK uses around 1 GB of memory, while the other solvers use around 25–30 GB of memory.

8.2 Case study 2 (Parallelization)

Here we show the effect of different tree branching on the parallelization, and, therefore, the solve times, of the algorithm. The problem statement is adapted from [43]. Consider a networked control system (NCS) consisting of a continuous-time LTI plant and a discrete-time controller that are connected through a communication network with induced sensor-to-controller (SC) delay, σ [44]. The full state of the system, x , is sampled by a sen-

sor with a constant sampling interval $T > 0$. The discrete-time controller is event-driven and able to monitor the SC delay, via timestamping. The discrete-time control signal u_k is transformed to a continuous-time control input $u(t)$ by a zero-order hold.

8.2.1 Sensor-to-controller delay

The SC delay is modeled as a discrete-time stochastic process σ with a.s. bounded paths in $[0, T]$ and the martingale property $\mathbb{E}[\sigma_{t+1} | \sigma_t] = \sigma_t$.

First, we consider a stochastic process, $(\phi_t)_t$, that takes values in $[0, 1]$. We assume $\phi_{t+1} | \phi_t \sim \text{Beta}(\zeta_t, \beta_t)$ and we choose $\zeta_t = \zeta_t(\phi_t)$ and $\beta_t = \beta_t(\phi_t)$ so that $\mathbb{E}[\phi_{t+1} | \phi_t] = \phi_t$ is satisfied; then, we define $\sigma_t = \phi_t T$.

We impose $\mathbb{E}[\phi_{t+1} | \phi_t] = \frac{\zeta_t}{\zeta_t + \beta_t} = \phi_t$, or, equivalently,

$$\frac{\zeta_t}{\beta_t} = \frac{\phi_t}{1 - \phi_t}. \quad (43)$$

To achieve this we assume $\zeta_t = \theta \phi_t$ and $\beta_t = \theta(1 - \phi_t)$, so that the above is automatically satisfied, and $\theta > 0$ is a free parameter. It can then be seen that $\text{Var}[\phi_{t+1} | \phi_t] = \frac{\phi_t(1 - \phi_t)}{\theta + 1}$. This means that a large θ leads to a small conditional variance. The unconditional variance is $\text{Var}[\phi_t] = \phi_0(1 - \phi_0)(1 - \tilde{\theta}^t)$, where $\tilde{\theta} = \frac{\theta}{\theta + 1}$, so $\text{Var}[\phi_t] \rightarrow \phi_0(1 - \phi_0)$ as $t \rightarrow \infty$.

Now, we construct a scenario tree by sampling ϕ , where the children of a node are equiprobable. In particular, having determined the value of ϕ^i of a node $i \in \text{nodes}(0, N - 1)$, we sample $\phi^{i+} \sim \text{Beta}(\theta \phi^i, \theta(1 - \phi^i))$, $\forall i_+ \in \text{ch}(i)$. That is, we split $[0, 1]$ into $|\text{ch}(i)|$ many intervals of equal length, and take their centers ι^{i+} . Then, ϕ^{i+} is the value of the quantile of the above Beta at ι^{i+} . For this case study we set $\phi^0 = 0.1$ and $\theta = 1$. An example of the scenario tree is shown in Figure 8.

8.2.2 System dynamics and constraints

The NCS model is

$$\dot{x}(t) = A_c x(t) + B_c u(t), \quad (44a)$$

$$u(t) = u_k, \quad t \in [kT + \sigma_k, (k+1)T + \sigma_{k+1}), \quad (44b)$$

where

$$A_c = I_{n_x} + \text{diag}(a), \quad a_i \stackrel{\text{iid}}{\sim} \mathcal{N}(0, 0.01), \quad (45a)$$

$$B_c = 0.1 \cdot 1_{n_x \times n_u}. \quad (45b)$$

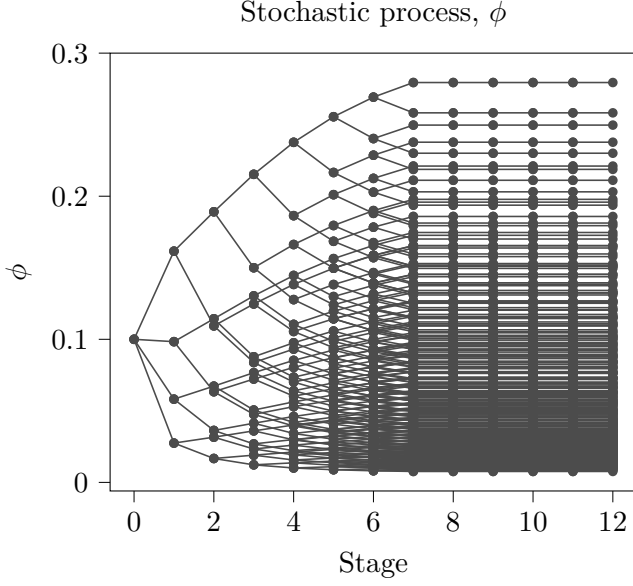


Figure 8: Example scenario tree of stochastic process, ϕ , where $\theta=1$ and $\phi^0=0.1$.

Using the technique described in [43], (44) is transformed into a discrete-time system of the form in (3) by letting the augmented system state be $\tilde{x}_k = [x_k^\top \ u_{k-1}^\top]^\top \in \mathbb{R}^{n_x+n_u}$ and $x_k = x(kT)$. That is,

$$\tilde{x}^i = A^i \tilde{x}^{i-} + B^i u^{i-} \quad (46)$$

where A^i and B^i are functions of A_c , B_c , and σ^i , following from [43, Eq. (5)]. The system is subject to discrete-time state, $\|x^i\|_\infty \leq 3, \forall i \in \text{nodes}(0, N)$, and input constraints $\|u^i\|_\infty \leq 0.9, \forall i \in \text{nodes}(0, N-1)$.

8.2.3 Cost

We use a quadratic stage cost function

$$\ell(\tilde{x}^i, u^i) = \tilde{x}^{i\top} Q \tilde{x}^i + u^{i\top} R u^i, \quad (47)$$

where $Q = \text{diag}(10^{-6} \cdot 1_{n_x+n_u})$ and $R = \text{diag}(0.1 \cdot 1_{n_u})$. We use a quadratic terminal cost function

$$\ell_N(\tilde{x}^j) = \tilde{x}^{j\top} Q_N \tilde{x}^j, \quad (48)$$

where $Q_N = \text{diag}([1_{n_x}^\top \ 10^{-6} \cdot 1_{n_u}^\top])$.

8.2.4 Performance

Here we investigate the effect of different tree branching on the parallelization of the algorithm, and so on the solve time. We also demonstrate the speedup of SPOCK over current state-of-the-art solvers. We set the horizon to $N = 48$, $n_x = 100$,

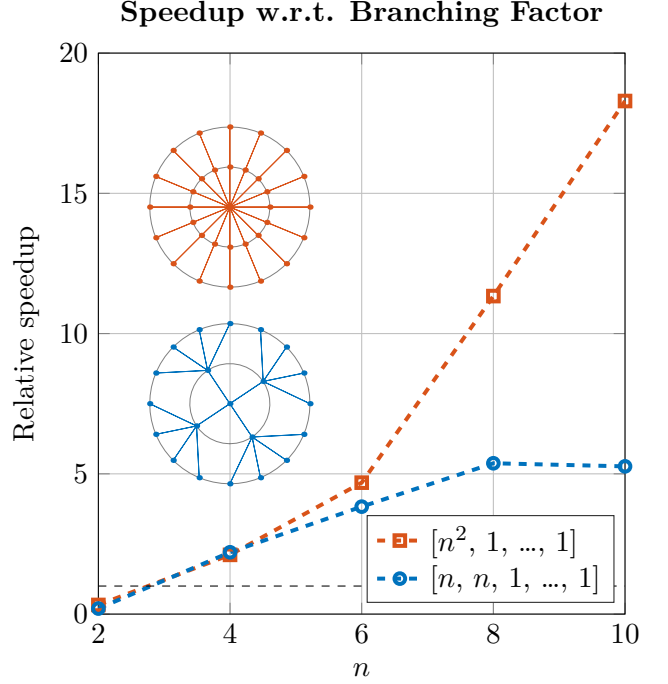


Figure 9: Speedup against problem size of GPU-accelerated SPOCK compared to the next fastest solver between MOSEK, GUROBI, IPOPT. We consider two distinct stage branching factors with the same number of scenarios, illustrated for the first two stages at $n = 4$.

$n_u = 50$, and the sampling time is $T = 5$. The risk measure is $\text{AV@R}_{0.95}$. The initial state and previous input are set element-wise to 2 and 0, respectively. Figure 9 demonstrates that a tree with a high initial branching (stage branching of $[n^2, 1, \dots, 1]$) is more amenable to parallelization than one with further branching (stage branching of $[n, n, 1, \dots, 1]$). Note that the algorithm step size α is the same for both cases due to preconditioning. Figure 9 further demonstrates the capability of SPOCK over MOSEK, GUROBI, and IPOPT with increasing speedup for wider problems (i.e., more scenarios).

9 Conclusions

This work demonstrates the feasibility and advantages of GPU acceleration for solving RAOCs. GPU-accelerated SPOCK significantly outperforms its serial counterpart and current state-of-the-art interior-point solvers, making it a strong candidate for real-time control applications with uncertain systems.

Acknowledgements

The authors gratefully acknowledge the invaluable guidance and support of Christian A. Hans, with Automation and Sensorics in Networked Systems Group, University of Kassel, Germany.

References

- [1] P. Sopasakis, D. Herceg, A. Bemporad, and P. Patrinos, “Risk-averse model predictive control,” *Automatica*, vol. 100, pp. 281–288, 2019.
- [2] C. A. Hans, P. Sopasakis, J. Raisch, C. Reincke-Collon, and P. Patrinos, “Risk-averse model predictive operation control of islanded microgrids,” *IEEE TCST*, vol. 28, no. 6, pp. 2136–2151, 2019.
- [3] Y. Chow, M. Ghavamzadeh, L. Janson, and M. Pavone, “Risk-constrained reinforcement learning with percentile risk criteria,” *JMLR*, vol. 18, no. 1, pp. 6070–6120, 2017.
- [4] Y. Chow, A. Tamar, S. Mannor, and M. Pavone, “Risk-sensitive and robust decision-making: A CVaR optimization approach,” *Adv. neural inf. proc. sys.*, vol. 28, 2015.
- [5] J. P. Maree, S. Gros, and V. Lakshmanan, “Low-complexity risk-averse MPC for EMS,” in *IEEE Smart Grid Comm*, IEEE, 2021, pp. 358–363.
- [6] G. Barsi Haberfeld, “Efficient algorithms for risk-averse air-ground rendezvous missions,” Ph.D. dissertation, University of Illinois at Urbana-Champaign, 2021.
- [7] A. Dixit, M. Ahmadi, and J. W. Burdick, “Risk-averse receding horizon motion planning,” *arXiv preprint arXiv:2204.09596*, 2022.
- [8] M. Schuurmans, A. Katriniok, H. E. Tseng, and P. Patrinos, “Learning-based risk-averse model predictive control for adaptive cruise control with stochastic driver models,” *IFAC-PapersOnLine*, vol. 53, no. 2, pp. 15 128–15 133, 2020.
- [9] E. Cinquemani, M. Agarwal, D. Chatterjee, and J. Lygeros, “Convexity and convex approximations of discrete-time stochastic control problems with constraints,” *Automatica*, vol. 47, no. 9, pp. 2082–2087, 2011.
- [10] J. B. Rawlings, D. Q. Mayne, and M. Diehl, *Model predictive control: theory, computation, and design*. Nob Hill Publishing Madison, WI, 2017, vol. 2.
- [11] D. Dentcheva and A. Ruszczyński, *Risk-Averse Optimization and Control: Theory and Methods*. Springer Nature, 2024.
- [12] Y. Wang and M. P. Chapman, “Risk-averse autonomous systems: A brief history and recent developments from the perspective of optimal control,” *Artificial Intelligence*, p. 103 743, 2022.
- [13] M. V. Pereira and L. M. Pinto, “Multi-stage stochastic optimization applied to energy planning,” *Mathematical programming*, vol. 52, no. 1, pp. 359–375, 1991.
- [14] A. Shapiro, “Analysis of stochastic dual dynamic programming method,” *EJOR*, vol. 209, no. 1, pp. 63–72, 2011.
- [15] B. F. P. da Costa and V. Leclère, “Dual SDDP for risk-averse multistage stochastic programs,” *arXiv preprint arXiv:2107.10930*, 2021.
- [16] A. Shapiro, W. Tekaya, J. P. da Costa, and M. P. Soares, “Risk neutral and risk averse stochastic dual dynamic programming method,” *EJOR*, vol. 224, no. 2, pp. 375–391, 2013.
- [17] P. Sopasakis, M. Schuurmans, and P. Patrinos, “Risk-averse risk-constrained optimal control,” in *ECC*, IEEE, 2019, pp. 375–380.
- [18] E. D. Andersen and K. D. Andersen, “The MOSEK interior point optimizer for linear programming: An implementation of the homogeneous algorithm,” in *High performance optimization*, Springer, 2000, pp. 197–232.
- [19] Gurobi Optimization, LLC, *Gurobi optimizer reference manual*, 2018.
- [20] A. Wächter and L. T. Biegler, “On the implementation of an interior-point filter line-search algorithm for large-scale nonlinear programming,” *Mathematical programming*, vol. 106, pp. 25–57, 2006.
- [21] A. S. Nemirovski and M. J. Todd, “Interior-point methods for optimization,” *Acta Numerica*, vol. 17, pp. 191–234, 2008.

- [22] R. Chowdhury and D. Subramani, “Optimal path planning of autonomous marine vehicles in stochastic dynamic ocean flows using a GPU-accelerated algorithm,” *IEEE Journal of Oceanic Engineering*, 2022.
- [23] A. K. Sampathirao, P. Sopasakis, A. Bemporad, and P. Patrinos, “Distributed solution of stochastic optimal control problems on GPUs,” in *CDC*, 2015, pp. 7183–7188.
- [24] A. Bodard, R. Moran, M. Schuurmans, P. Patrinos, and P. Sopasakis, “SPOCK: A proximal method for multistage risk-averse optimal control problems,” *IFAC-PapersOnLine*, vol. 56, no. 2, pp. 1944–1951, 2023, 22nd IFAC World Congress, ISSN: 2405-8963.
- [25] A. Chambolle and T. Pock, “A first-order primal-dual algorithm for convex problems with applications to imaging,” *Journal of mathematical imaging and vision*, vol. 40, no. 1, pp. 120–145, 2011.
- [26] A. Themelis and P. Patrinos, “SuperMann: A superlinearly convergent algorithm for finding fixed points of nonexpansive operators,” *IEEE TACON*, vol. 64, no. 12, pp. 4875–4890, 2019.
- [27] D. G. Anderson, “Iterative procedures for nonlinear integral equations,” *JACM*, vol. 12, no. 4, pp. 547–560, 1965.
- [28] J. Bezanson, A. Edelman, S. Karpinski, and V. B. Shah, “Julia: A fresh approach to numerical computing,” *SIAM Review*, vol. 59, no. 1, pp. 65–98, 2017.
- [29] K. Høyland and S. W. Wallace, “Generating scenario trees for multistage decision problems,” *Management science*, vol. 47, no. 2, pp. 295–307, 2001.
- [30] J. Dupačová, G. Consigli, and S. W. Wallace, “Scenarios for multistage stochastic programs,” *Annals of operations research*, vol. 100, no. 1, pp. 25–53, 2000.
- [31] R. G. Gallager, *Stochastic processes: theory for applications*. Cambridge University Press, 2013.
- [32] A. Shapiro, D. Dentcheva, and A. Ruszczyński, *Lectures on stochastic programming: modeling and theory*. SIAM, 2021.
- [33] R. T. Rockafellar, S. Uryasev, *et al.*, “Optimization of conditional value-at-risk,” *Journal of risk*, vol. 2, pp. 21–42, 2000.
- [34] E. K. Ryu and S. Boyd, “Primer on monotone operator methods,” *Appl. Comput. Math*, vol. 15, no. 1, pp. 3–43, 2016.
- [35] R. T. Rockafellar and R. J.-B. Wets, *Variational Analysis*, 3rd. Berlin, Heidelberg: Springer, 2009.
- [36] T. Pock and A. Chambolle, “Diagonal preconditioning for first order primal-dual algorithms in convex optimization,” in *2011 International Conference on Computer Vision*, IEEE, 2011, pp. 1762–1769.
- [37] NVIDIA Corporation, *CUDA C++ Best Practices Guide*, 2020.
- [38] NVIDIA Corporation, *CUDA C++ Programming Guide*, 2020.
- [39] S.-F. Hsieh, K. R. Liu, and K. Yao, “A unified square-root-free approach for QRD-based recursive-least-squares estimation,” *IEEE Transactions on Signal Processing*, vol. 41, no. 3, pp. 1405–1409, 1993.
- [40] R. Moran and P. Sopasakis, *GPUtils*, [Online] Available: github.com/GPUEngineering/GPUtils, Accessed: 1 Mar 2025.
- [41] B. Stellato, G. Banjac, P. Goulart, A. Bemporad, and S. Boyd, “OSQP: An operator splitting solver for quadratic programs,” *Mathematical Programming Computation*, vol. 12, no. 4, pp. 637–672, 2020.
- [42] E. D. Dolan and J. J. Moré, “Benchmarking optimization software with performance profiles,” *Mathematical programming*, vol. 91, pp. 201–213, 2002.
- [43] P. Patrinos, P. Sopasakis, and H. Sarimveis, “Stochastic model predictive control for constrained networked control systems with random time delay,” *IFAC Proceedings Volumes*, vol. 44, no. 1, pp. 12 626–12 631, 2011.
- [44] M. Posthumus-Cloosterman, “Control over communication networks: Modeling, analysis, and synthesis,” Ph.D. dissertation, Eindhoven University of Technology (TU/e), 2008.